Multi-Classification of Chest X-Ray Images Using an Enhanced Deep Learning Approach

Revathi Annam
Department of Computer Science and Engineering
Koneru Lakshmaiah Education Foundation, Hyderabad, Telangana-500075, India
Department of Information Technology, Vallurupalli Nageswara Rao Vignana Institute of Engineering and Technology, Hyderabad, Telangana-500090, India
revathi_a@vnrvjiet.in

Savadam Balaji
Department of Computer Science and Engineering
Koneru Lakshmaiah Education Foundation, Hyderabad, Telangana-500075, India
balajis@klh.edu.in

Abstract: *Millions of people have died as a result of several epidemic lung diseases that have spread around the world, including COVID-19, lung opacity, and pneumonia. because these disorders exhibit small changes in Chest X-Ray (CXR) images, medical specialists have had difficulty in accurately diagnosing them. This research proposes a computer-aided lung disease detection technique based on CXR images to assist medical professionals. To meet the demand for practical and user-friendly diagnostic instruments, this research introduces new, enhanced deep-learning models designed explicitly for multi-class diagnosis of lung diseases, including normal, viral pneumonia, tuberculosis, lung opacity, fibrosis, and COVID-19 pneumonia, using CXR images. The four major phases of the proposed research are pre-processing, feature extraction, classification, and segmentation. First, the pre-processing phase employs a gaussian filtering approach to reduce input noise, thereby enhancing the image quality. Then, in the feature extraction stage, a custom Convolutional Neural Network (CNN) model is utilized to extract useful features and mitigate complexity problems. After feature extraction, the multiple classes of lung diseases are effectively classified by using the Enhanced ResNet50V2 (EResNet50V2) model. The region of infection in the chest radiographs is accurately identified and delineated using the Enhanced DeepLabV3+(EDeepLabV3+) model. The efficacy of the proposed approach is evaluated through extensive experiments against existing state-of-the-art methods. The research's results demonstrated exceptional accuracy, with a 99.47% success rate. Throughout the six-class classification system, the average performance metrics for F1-score, recall, precision, Area Under the Curve (AUC), Intersection Over Union (IOU), and Dice Similarity Coefficient (DSC) were 0.9933, 0.9933, 0.9983, 0.9905, 0.9754, and 0.9867. This research advances the field of medical imaging and lays the foundation for developing deep learning-based systems for diagnosing lung diseases in the future*.

Keywords: *Lung diseases, CXR images, gaussian filtering, enhanced resnet50v2, and enhanced deeplabv3+*.

Received September 04, 2024; accepted November 11, 2025.
https://doi.org/10.34028/iajit/23/3/11

1. Introduction

Pneumonia, pulmonary fibrosis, chronic bronchitis, emphysema, and other illnesses can all contribute to lung disease, this is among the most deadly diseases a person can have. Furthermore, non-smokers are equally susceptible to lung ailments, which are mostly brought on by smoking [1]. This disease currently affects a large number of people, particularly in industrialized and developing nations. According to recent statistics, air pollution causes lung disorders, including asthma and Pneumonia, which increase the mortality rate [23]. Therefore, it's critical to identify lung-related diseases early to stop the rise in high death rates [46]. Several recent studies have demonstrated that lung segmentation can be accomplished effectively by using Chest X-Ray (CXR) images [18]. However, it requires considerable effort and time to isolate abnormal lung characteristics from the thoracic backdrop. A significant amount of medical resources is needed for the manual detection of lung diseases [40].

Modern medical technologies have enabled doctors to work more accurately and provide efficient clinical support [21]. The most popular method for identifying lung conditions is the use of CXR images, which are also a useful tool for determining the severity of the condition [22]. As a result, CXR images are used to diagnose lung diseases, and radiologists are employed to analyze them [38]. However, significant human error could occur if the CXR is incorrectly evaluated due to intricate and undetectable abnormalities in the lung tissues [14]. The most widely used kind of Computer-Aided Diagnosis (CAD) helps radiologists make decisions with less inaccuracy [37]. However, internal image suppression and high noise frequently degrade the CAD system's performance. Advanced disease detection methods must be incorporated into the CAD system to address this issue and lower mistakes and other classification complications [12].

Because deep learning and machine learning-based AI-driven methods outperform traditional healthcare analysis, researchers nowadays tend to favor them for

disease prediction [34]. For efficient lung disease classification, machine learning methods such as Artificial Neural Networks (ANN), Logistic Regression (LR), Decision Trees (DT), Random Forests (RF), and Support Vector Machines (SVM) are utilized by Mutukuru *et al.* [27]. However, when processing a larger dataset, machine-learning approaches lose some of their flexibility [47]. Additionally, due to difficulties with overfitting and data redundancy, it resulted in higher error rates The deep learning technique was introduced, which eliminates all of the shortcomings of the machine learning technique and results in exceptional disease categorization performance [26, 56]. The features are automatically learned by deep learning methods, and this approach is also suitable for larger datasets. These are significant benefits of deep learning models [3]. Numerous previous studies have demonstrated the effectiveness of deep learning-based methods for classifying lung diseases [16]. Novel deep-learning approaches have been used in published studies to classify lung disorders, including infiltration, effusion, cardiomegaly, emphysema, edema, fibrosis, pneumonia, and hernia [33]. On the other hand, because visual discrepancies are more reliable, their performance is diminished. Additionally, the shortcomings of the previous models for classifying lung diseases prevent them from making multi-class classifications [44]. In lung disease detection, existing models have exacerbated the complexity problem when executing multi-class classification tasks. Furthermore, during training, existing deep-learning models often struggle to handle multiple classes of images effectively [53]. As a result, there are problems with over-fitting and a decrease in detection accuracy. This research presents a novel enhanced deep learning framework that employs CXR images to categorize lung tumor diseases and addresses these issues with existing deep learning models. To improve lung disease detection performance, a deep Enhanced Residual Network 50 Version 2 (EResNet50V2) model and an Enhanced DeepLab Version 3 Plus (EDeepLabV3+) model are hybridized in this proposed model for classification and segmentation. The proposed model's increased efficiency allows it to handle various input sample classes and minimize complexity by applying an Adam optimization algorithm to fine-tune the parameters. Additionally, the proposed research utilizes a custom Convolutional Neural Network (CNN) model to extract significant features, which can enhance the effectiveness of classification.

Motivation: The most dangerous and deadly disease that might potentially result in death for a person is lung disease. Every year, the death rate might rise by as much as five million, especially in countries that are developing and developed. The lung is regarded as a vital respiratory organ and is very vulnerable to infections from the outside and within. The majority of lung ailments are caused by physical diseases, air pollution, and micro- and macro-biological infections. To reduce the death rate, lung disorders must be identified early. Manual methods require a significant amount of time and are quite challenging. Typically, CXR images are effective in detecting lung disease; however, they have a significant error rate because they do not clearly show thoracic structures. In the lung CXR images, to quickly and accurately detect any abnormalities, the CAD system processes the CXR images. However, processing larger CXR images frequently causes the CAD system to malfunction. These significant drawbacks necessitate the development of advanced methods for integrating with the CAD system, enabling the accurate identification of lung diseases. For classifying lung diseases, the purpose of this research is to use extracted lung features to create deep-learning models.

The following representations show the proposed method's primary contribution:

- Using the CXR image dataset, we propose a novel enhanced deep learning model (EResNet50V2-EDeepLabV3+) for lung disease classification and segmentation, aiming to improve detection accuracy.
- To emphasize a Gaussian filtering-based noise removal technique, the image's visual quality is enhanced efficiently. Then, conventional data augmentation techniques are applied to increase the number of images in the dataset.
- To present a new Custom CNN (CCNN) based feature extraction method that reduces complexity by extracting multi-level features.
- To propose the EResNet50V2 model to categorize lung disease precisely.
- To propose the EDeepLabV3+ model for segmenting the infected region of lung diseases properly.
- To enhance the effectiveness of the proposed models for classification and segmentation, the Adam optimizer is employed to fine-tune the network parameters.
- To demonstrate the efficacy of the proposed approach in comparison to other pertinent lung disease system approaches, it is necessary to validate its performance under various performance measures.

The sections that follow are arranged as follows: section 2 examines the recent publications on lung disease classification. The proposed methodology for diagnosing lung diseases from the provided input samples is covered in section 3. To demonstrate the effectiveness of the proposed research, section 4 conducts a comparison analysis with other previous studies and provides the findings and discussion of the recommended model. Section 5 provides a comprehensive summary of the proposed research, along with practical recommendations for the future.

2. Related Prior Works

Recent years have seen several research works employing various deep learning and machine learning algorithms to diagnose lung diseases based on CXR images. Thus, we looked over several studies in which scientists used X-ray images to investigate various classification techniques. All the investigations, however, are illustrated in this section. To identify common lung disorders, Arora *et al*. [4] present a classification model Multiple Lung Disease Classification (MLDC) for classifying multiple lung diseases. A Quantum Classifier (QC) and an ANN are two classifiers that were introduced with an MLDC feature extraction model. It was composed of two modules for classification and one module for feature extraction. Two classifiers have been proposed: MLDC-QC, which is an Multi-Multi-Single (MMS)-QC, and MLDC-ANN, which is a fully connected neural network. Based on quantum classifiers and classical CNN models, a hybrid respiratory lung disease diagnosis framework was developed by Rao *et al*. [31]. It integrates quantum classifiers with a classical deep feature extraction model. The feature extraction process was done by using a CNN model. Additionally, two quantum machine learning algorithms, including Multi-Single-Multi-Single (MSMS) and Multi-Multi-Single (MMS) were introduced. A quantum variational circuit with measurement, entanglement, and encoding features was used to construct these two quantum classifiers.

For the classification of multi-class lung diseases, a CNN model optimized with the grid search technique was introduced by Ashwini *et al*. [5]. This research uses two separate models, classification_1 and classification_2. While classification_2 categorizes multiple lung diseases, the classification_1 model detects lung diseases.

A different model using deep learning was developed by Verma *et al*. [48] for classifying lung diseases. The pre-processing of all CXR images primarily involves segmenting them using a U-Net architecture and using the histogram equalization approach over the median filter. The pre-processed CXR images are then used to extract features using a VGG-16 model. Using a synthetic minority oversampling technique, a balanced dataset is formed, and the samples are then further sampled. With 10-fold cross-validation, an SVM classifier is used to classify the class-balanced features. A different deep-learning system, called CX-RaysNet, was introduced by Ali *et al*. [2] to identify various types of lung diseases using CXR images automatically. The primary innovation of the CX-RaysNet architecture was the combination of a group of convolutional layers, as well as the use of dropout regularization and small filter sizes. This occurrence enhances the model's ability to identify subtle details that indicate various lung diseases.

Upon a thorough examination of all the literature, it is evident that appropriate and optimal feature extraction techniques, augmentation methods, and image pre-processing methods are not widely applied to massive data hubs. Additionally, their methodology yielded a limited number of class categories and low accuracy in multi-class categorization. Nevertheless, Table 1 lists each drawback of the previous research on categorizing lung diseases. We have addressed the numerous significant constraints of their work by introducing a variety of cutting-edge techniques to significantly increase image categorization accuracy. Below is a detailed description of each process for ease of use.

Table 1. Comparative analysis of traditional techniques for multi-class lung disease classification.

Reference	Year	Categories	Method	Accuracy	Merits	Demerits
Arora *et al*. [4]	2024	COVID-19, pneumonia, tuberculosis, and normal	Quantum classifier	97.50%	High accuracy and a reduction of gradient insufficiencies	1. Lack of knowledge regarding the best attributes 2. Complicates time more and causes issues with data redundancy.
Rao *et al*. [31]	2024	COVID-19, viral, and normal	IBMQ-QASM	98.10%	1. Easy and inexpensive method. 2. It generates effective categorization outcomes.	1. The restricted quantity of images 2. Absence of noise and removal of overlay text from images
Ashwini *et al*. [5]	2024	COVID-19, lung opacity, pneumonia, and lung cancer	CNN	99.82%	1. Increased precision, and most problems are resolved. 2. Achieved efficient results with less time complexity.	The lack of optimal feature extraction has a minor negative impact on efficiency, but this issue will be addressed in the future.
Verma *et al*. [48]	2024	COVID-19, viral pneumonia, and normal	SVM	98%	1. It works well in real-world settings 2. It generates better performance results for the classification of lung diseases.	1. Lack of knowledge about the best attributes. 2. Unbalanced datasets may cause them to suffer since they can become biased in favor of the majority class.
Ali *et al*. [2]	2024	COVID, viral pneumonia, normal, and opacity	CX-RaysNet	97.25%	Achieved efficient results with less time complexity	1. Complexity of time using CXR images. 2. To tune the hyper-parameters of this model, a significant amount of labelled data, a powerful computer, and an optimization technique are needed.

2.1. Problem Statement

Upon thorough examination of the numerous published research, several intricacies are identified in the process of accurately classifying lung diseases. From the CXR images, the accuracy performance is reduced by the noise in the images obtained. In the CXR images, the existing research works are unable to generate a pre-processing step that effectively removes noise. The created model's overall performance and classification accuracy are lowered by this. Additionally, some existing approaches take longer to complete classification tasks due to more complex problems. This problem causes a high error rate and has a direct impact on the classification model's performance. Therefore, it's essential to lessen the complexity problem by speeding up the procedure of lung disease identification. Furthermore, the low efficiency of the existing approaches makes managing an enormous amount of input images challenging. Thus, even with a large dataset as input, existing approaches are unable to achieve higher performance. Additionally, it is crucial to extract relevant features to enhance the accuracy of lung disease identification. However, due to their limited learning capacity, the existing approaches were unable to extract enough features. Therefore, the proposed research introduces an automated, efficient, and enhanced deep learning model to address the existing challenges.

The existing research papers focus on binary categorization, including the detection of Pneumonia, COVID-19, and healthy CXR images. This necessitates the development of a model that can classify among different lung diseases. To create such a model, we require a training dataset comprising CXR images of various lung conditions. To the best of our knowledge, there are no multi-class CXR images available for lung disorders. This inspired us to create a common dataset that can be utilized to identify a variety of lung diseases. Therefore, a multi-class Lung Disease Dataset (LDD) has been created.

3. Methodology

Since multi-class lung diseases have higher severities and are thought to be the most frequent disease worldwide, their detection is more complicated. Numerous models for feature extraction and classification related to lung diseases have been investigated in earlier research. Nevertheless, these methods suffer from a significant overfitting issue, which reduces recognition accuracy. Throughout the classification process, the accuracy of the abnormal class declines, while the accuracy of the normal class remains unique. The recommended method overcomes all the issues of the existing techniques and improves the classification performance. The workflow of the proposed approach is depicted in Figure 1 for lung disease classification and segmentation.

From the Kaggle repository, the CXR image dataset was gathered, and it is used to identify lung diseases. Then, the CXR image's quality is enhanced by applying a Gaussian filtering-based pre-processing technique for noise reduction. Then, the dataset images are balanced by adjusting the number of images in each class using conventional data augmentation techniques, such as rotation, reflection, and shearing. Then, a Custom Convolutional Neural Network (CCNN) model is introduced in the feature extraction process for extracting multi-level features. After feature extraction, these extracted features are given to the EResNet50V2 model for detecting lung diseases. Then, to precisely identify and delineate the region of infection in the classified lung diseases, the EDeepLabV3+ model is used. The hyperparameters of the proposed network models are optimized using the Adam optimizer to enhance network performance.

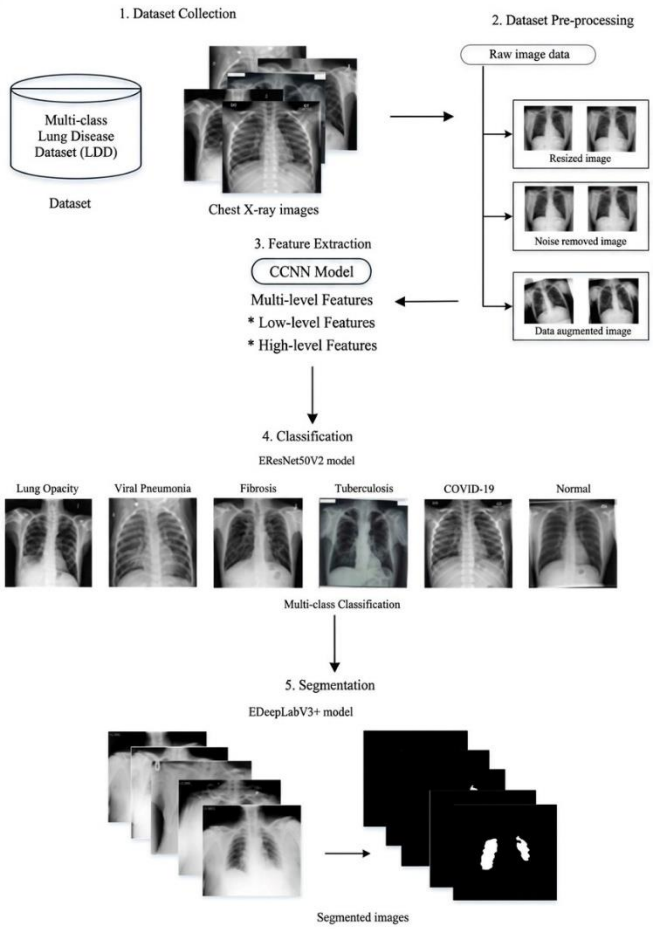

Figure 1. The detailed workflow visual representation of the proposed enhanced deep learning models.

3.1. Database Description

The COVID-19 radiography database [10] served as the main experimental collection for our research. There are 21,165 CXR images in this extensive collection, covering a wide variety of cases. The COVID-19 cases comprise 3,616 images, 10,192 images represent normal lung conditions, and images of viral pneumonia total

1,345. To further expand the scope of our research, we also included images from the National Institutes of Health Chest X-ray (NIH CXR) dataset [13], which represented fibrosis (1,686 images) and tuberculosis (3,500 images). By incorporating more cases, our collection becomes more varied and all-encompassing. Figure 2 shows a representative sample of this extensive CXR collection, highlighting the range of cases and conditions covered in our research. Our deep learning model is trained and evaluated using this varied dataset, which helps to ensure that it is reliable and efficient in identifying a variety of pulmonary diseases.

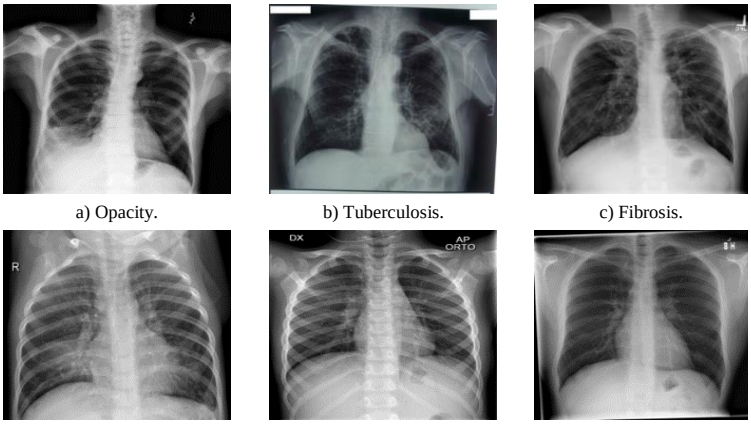

a) Opacity. b) Tuberculosis. c) Fibrosis.

d) Pneumonia. e) COVID. f) Normal.

Figure 2. Sample images of each class from the given dataset.

Figure 2 shows an example of a typical case along with six diseases that can cause harm to the lungs. Areas of higher radio density in Figure 2-a) indicates the presence of an opacity. There are areas in this image where the lung fields' typically translucent appearance is hidden, suggesting an obstruction to the flow of X-rays caused by cells, fluid, or other materials. Here is a tuberculosis case from Figure 2-b). often appearing as distinct nodules, the upper lobes of the lungs are mainly affected by tuberculosis. Figure 2-c). shows Fibrosis, which is characterized by a reticular pattern, the fibrotic process has caused the lung architecture to seem deformed and retracted. This can result in a structure that resembles honeycombs, with fibrous tissue encircling small cystic areas. A viral infection of the lungs is depicted in Figure 2-d). This infection can manifest as a more widespread, bilateral interstitial pattern. As a result, all of the lung fields may appear fuzzy rather than having a single, prominent consolidation concentration, which is frequently more noticeable near the lungs' periphery. The COVID-19 virus is shown in Figure 2-e). This virus usually manifests as bilateral peripheral ground-glass opacities. Additionally, on the ground-glass opacities, it can feature a consolidation pattern with interlobular septal thickening superimposed. Figure 2-f) shows a typical lung X-ray that can be used as a reference for comparing abnormal images. Sharp costophrenic angles, well-defined diaphragms, and clear lung fields free of aberrant opacification are all present, indicating the lack of disease.

3.2. Collection Splitting

In this section, we separated the data into two more segments: the first 65% was utilized directly for training, and the second 15% was reserved for validation. The correctness and dependability of deep learning models are ensured through the use of a validation phase. 20% of the total data was set aside for testing, an essential step in assessing how well deep learning models perform in settings that resemble real-world situations [25]. Table 2 provides a detailed illustration of the data distribution across different training, validation, and testing segments.

Table 2. The collection of data.

Class name	Training	Testing	Validation
Normal	6516	2047	1629
COVID	2291	753	572
Viral pneumonia	867	262	216
Opacity	3833	1221	958
Fibrosis	1094	318	274
Tuberculosis	2264	670	566
Total	16,865	5271	4215

3.3. Data Pre-processing

This section describes the image pre-processing methods utilized in this model. Pre-processing images is essential to ensuring that they work with the CNN architecture. Initially, each image is cropped to a consistent 224×224-pixel size in the collection. This standardization is essential since larger images can obscure important characteristics required for a precise diagnosis. Pixel values in each image are adjusted to fall between 0 and 1 after the resizing process. To improve CNN's capacity to process the input images efficiently, this normalization phase is essential.

First, a Gaussian filter is used to reduce the noise in the images. The Gaussian filter is employed because it can efficiently decrease noise while preserving the

image's details. After that, more dataset photos are added using standard data augmentation methods. Additionally, image augmentation methods are employed to address the issue of the limited number of images in the training set and enhance training effectiveness. Several modifications are used in these methods to increase the size of the training set. Except for normal lung conditions and lung opacities, we have employed several data augmentation strategies in our research to enhance the quality of the training set.

3.3.1. Noise Removing

The proposed research employs a Gaussian filter to minimize noise in the CXR images and enhance visual quality. The Gaussian filter is a widely used image processing technique for reducing noise and blurring, while still preserving essential image structures [50]. It operates by convolving the image with a Gaussian kernel, where pixels nearer to the kernel's center are given higher weights compared to those farther away. This weighting mechanism produces a smoothing effect that suppresses high-frequency noise while preserving the structural integrity of anatomical regions. The degree of smoothing is controlled by the standard deviation of the Gaussian distribution (σ), with larger values yielding more substantial smoothing effects. Figure 3 illustrates sample images after noise elimination using the Gaussian filter.

$$G(x,y) = \frac{1}{2\pi\sigma^2} e^{\frac{z^2+y^2}{2\sigma^2}} \quad (1)$$

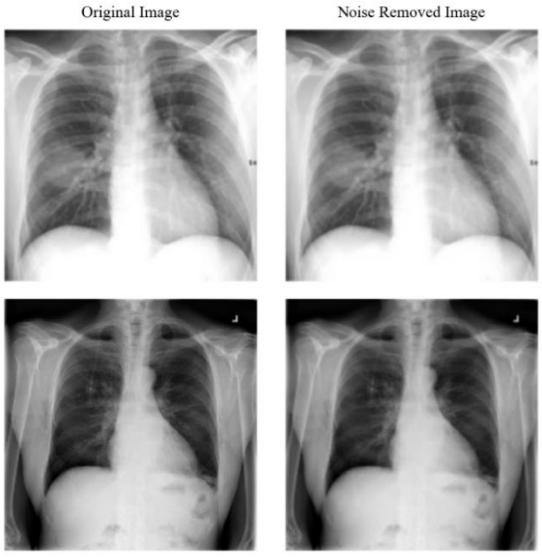

Figure 3. The sample of noise-removed images.

3.3.2. Data Augmentation

The practice of updating the training image collection to add more images for training is known as data augmentation. We have employed position augmentation in this research [15]. The reflection, rotation, and shear values of the image are included in the position augmentation and are listed in Table 3. The data-augmentation example is displayed in Figure. 4. The original CXR image can be seen in Figure 4-a). The horizontally reversed image is displayed in the Figure. 4-b). Random shear [-0.05 0.05] in Figure 4-c) shear image. A randomly rotated image with a [−5, 5] rotation is shown in the Figure 4-d). After data augmentation, the number of images is displayed in Table 4.

Table 3. Data augmentation.

Process	Quantity
Random Xshear	1
Random reflection	1
Random Rotation	−5 to 5
Random Yshear	1

Table 4. The image distribution after data augmentation.

Condition	Training (65%)	Validation (15%)	Testing (20%)
Viral Pneumonia	4371	1009	1345
COVID	4701	1085	1447
Tuberculosis	4550	1050	1400
Fibrosis	5485	1265	1686
Normal	6516	1629	2047

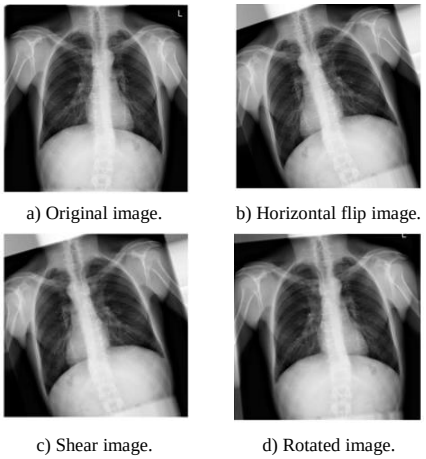

a) Original image. b) Horizontal flip image.

c) Shear image. d) Rotated image.

Figure 4. The resulting images after applying various data augmentation techniques.

3.4. Multi-level Feature Extraction

In this research, the high-level and low-level features are extracted by using a CCNN [32]. The low-level and high-level features, such as edge features, histogram features, shape features, Region of Interest (ROI) Features, texture and pattern features, and global contextual features, are effectively extracted to enhance the classification accuracy of the proposed research.

The proposed feature extraction method comprises two fully connected layers, three max-pooling layers, and three convolutional layers. The filters in this architecture are 64, 64, and 32, and the kernel dimension and stride are both (2×2). By using kernels to perform convolution operations on input features, the convolutional layer can extract crucial and reliable characteristics from the scan images. In this architecture, the activation function is the Rectified Linear Unit (ReLU) transformation function. For any negative input, the function above returns 0; for any positive input, it returns the same value as the input. The most significant and helpful information is found and

processed by the max-pooling layer, which reduces computation. The pre-processed CXR images are sent to the feature extraction module or a Custom CNN model for each data sample. The structure of the CCNN model is shown in Figure 5.

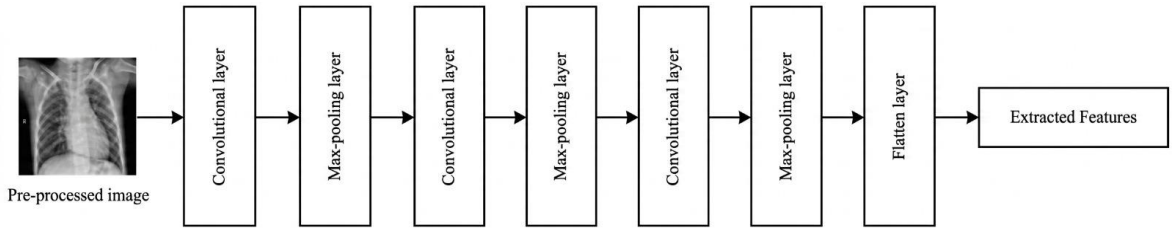

Figure 5. The CCNN model structure.

3.5. Classification

The existing models for classification are labor-intensive, intrusive, and vulnerable to human error. For classifying lung diseases, these drawbacks make the use of a fully automated method imperative. The goal of this research is to develop an EResNet50V2 model for the multi-classification of lung diseases. The addition of max pooling, batch normalization, and dropout layers has improved the accuracy of the conventional model. The activations of the layer before it are normalized using batch normalization, which involves scaling and altering the results to obtain a zero mean and unit variance. By adjusting the scale factor, this is accomplished. As a result, the model's stability is enhanced, training is accelerated, the impact of internal covariate shift is reduced, and its generalization performance is improved. By decreasing the model parameters, max pooling helps to improve the computational efficiency of the model. Conversely, dropout lessens over-fitting by lowering the co-adaptation between neurons. Consequently, this compels the network to develop stronger and more broadly applicable features. These modifications allowed the proposed model to achieve a greater classification accuracy.

Determining the type of tumor that can be visible in the CXR image with a high degree of precision is the classification's objective. To train a CNN for the classification of chest disorders, a sizable collection of CXR images and their corresponding labels, which specify the type and presence of the tumor, is required.

3.5.1. Enhanced ResNet50V2 Model

ResNet50V2, a CNN architecture [41], is utilized in the proposed framework to aid in image classification. It is an adaptation of the ResNet50 framework, which was initially made available in 2015. With 50 layers, the ResNet50V2 architecture utilizes skip connections to prevent the network from encountering the vanishing gradient issue when learning deeper representations. It is possible to connect the input of a layer that is two or three layers down in the network to the output of another layer by using skip connections. This enables data to bypass layers that would otherwise result in an excessively narrow gradient during backpropagation, which could impede or even prevent learning from occurring.

One of the most significant new aspects of ResNet50V2 is that it employs an architecture known as a "bottleneck" in several of its layers. ResNet50V2 also utilizes weight decay, activation functions, and identity mappings, among other methods, to enhance performance. The structure of the residual block consists of a skip connection and three convolutional layers. Each block comprises several layers, and the skip connections enable the network to acquire more complex representations without encountering the vanishing gradient issue.

- **Input layer**: after receiving the input image, the input layer performs some simple pre-processing, including normalization.
- **Convolutional layer**: the first layer, a 7×7 layer with a stride of 2, applies 64 filters to the input image using convolutional layers. The spatial dimensions of the image are reduced by this layer, but the overall number of channels is increased concurrently.
- **Max pooling layer**: a single max pooling layer with a 3×3 pool size and a stride of 2 can help regulate the spatial dimensions of the output from the first convolutional layer.

The fundamental building block of the ResNet50V2 architecture is composed of 16 different types of residual blocks. Each leftover material block has a distinct structure: 1×1 convolutions are employed in the first layer of each residual block to reduce the overall number of channels in the intake.

The decreased input is filtered using a 3×3 convolution in the second layer. Another 1×1 convolution in the third layer increases the number of channels to the initial number. The output of the third layer is combined with the input from the beginning of the process to create the ultimate result of the residual block.

Additionally, each residual block features skip connections, which enable the network to acquire deeper representations without encountering the vanishing gradient problem by skipping one or more levels.

- **Global Average Pooling Layer**: the result of the last residual block, for example, is condensed into a single vector by a global average pooling layer, reducing its spatial dimensions.
- **Fully Connected Layer**: after applying a weight matrix to the output of the global average pooling layer, a fully connected layer will use that output to build the final network result.

The addition of dropout, max-pooling, and batch normalization layers improves the standard ResNet model. Figure 6 shows the structure of the EResNet50V2 model; Figure 7 shows the structures of Blocks 1, 2, and 3. The use of batch normalization has reduced the number of iterations required to attain convergence, which has substantially speed up the training of anything similar to the proposed methodology. This is because it mitigates the vanishing gradient problem, which could cause the learning process to stop altogether. Batch normalization makes it easier to tune the network's weights by keeping activations within a specific range, as it normalizes the inputs to each layer. It strengthened the resistance of deep neural network training against initialization effects by reducing the degree to which the network relied on the initial values of its weights. This is because normalization helps reduce the variance in the inputs delivered to each layer, making the network more stable and easier to optimize. As a result of the effects of overfitting being mitigated, the generalization functionality of deep neural networks was significantly improved. Batch normalization can aid in regularizing the network by reducing the internal covariate shift, which in turn lessens the probability of overfitting.

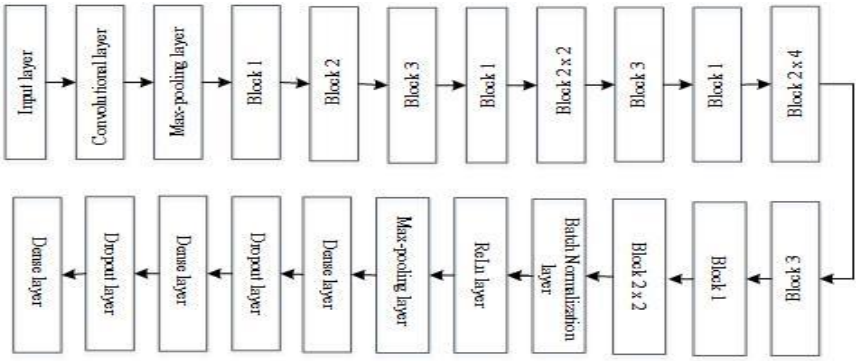

Figure 6. The structure of the EResNet50V2 model.

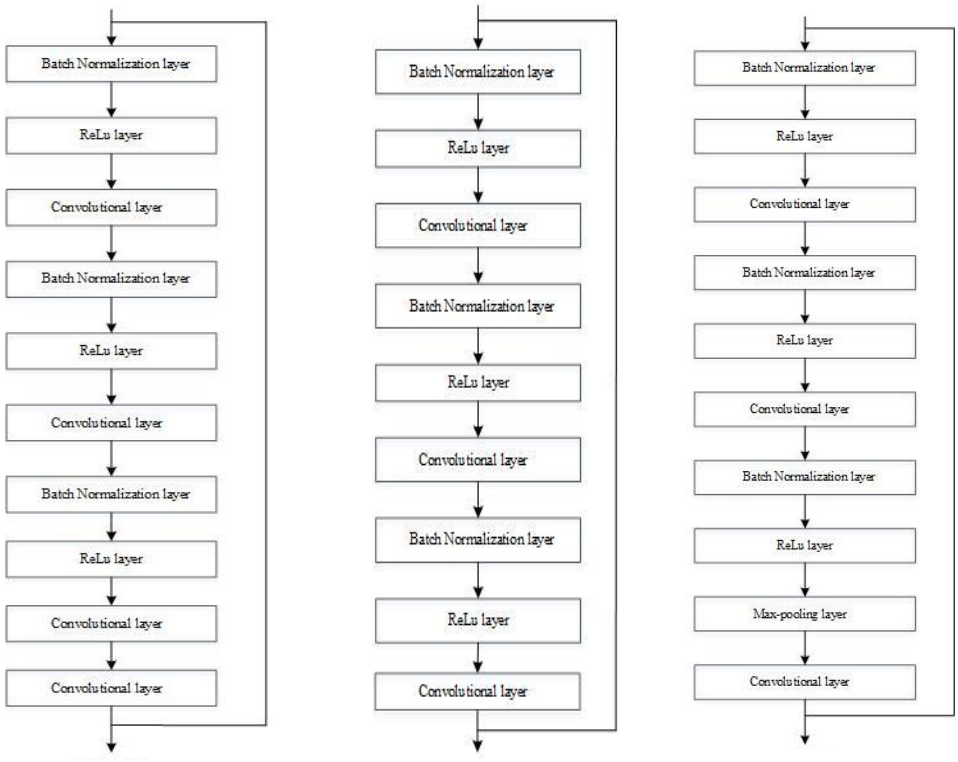

a) Block 1. b) Block 2. c) Block 3.

Figure 7. The structure of blocks.

By selecting the most excellent value in each pooling zone, max-pooling can reduce the size of the feature maps. Consequently, this reduced both the number of parameters in the network and the computational load

on the successive layers. Reducing the parameter range helped prevent over-fitting, which was a further advantage. It selects the highest activation level inside each pooling zone to achieve this. As a result, the network has some translational invariance. This indicates the network is less susceptible to small translations of the input image, which could enhance the network's generalization capabilities.

Dropouts are regularization strategies that help keep neural networks from becoming overly intelligent. Neural network training is performed using the dropout technique, which functions by randomly deleting units from the network. This allows the remaining units to acquire more resilient features that are less dependent on particular inputs. As a result, the network's generalization performance improved, and the probability of overfitting decreased. Additionally, by requiring every unit in the network to acquire valuable qualities independently, it decreased co-adaptation between units. As a result, the network's learnt features were more diverse and less susceptible to slight variations in the input.

3.6. Lung Disease Segmentation

The affected regions of lung diseases are properly segmented using the EDeepLabV3+ model for early-stage lung disease diagnosis.

For medical image segmentation, various deep learning models, such as UNet [19] and UNet++ [49], FasterNet [51], and Bidirectional Long Short-Term Memory (BiLSTM) [8], are employed in existing papers. Although these models produce higher results, they have some limitations. Accurate segmentation depends on capturing contextual information from broader regions of the image, which the existing segmentation approach may fail to accomplish. During training, the network may encounter vanishing gradient problems, which can hinder its ability to learn long-range dependencies. The U-Net model may struggle to precisely segment items with complex, irregular boundaries because it may not be able to capture all the fine-grained information required. The existing segmentation models dramatically increase memory needs and computational complexity.

To overcome the problems, we have utilized the backbone of the DeepLabV3+ model [43] for lung disease segmentation in this research. Using atrous (dilated) convolution, the DeepLabV3+ efficiently expands the receptive field while maintaining resolution and avoiding the need for additional parameters. This solves the limited receptive field problem in UNet and UNet++ by enabling the model to capture additional contextual information. Atrous convolution is more effective in segmenting objects with irregular shapes because it preserves fine details and captures complex object boundaries.

The objective of the EDeepLabV3+ model is to more rapidly, precisely, and efficiently identify the interested impacted region in CXR pictures. By simplifying the Xception backbone network, training time is decreased; the sensory field is strengthened after the Atrous Spatial Pyramid Pooling (ASPP) [29] module, which captures contextual information, and is enhanced by adding the Enhanced Convolutional Block Attention Module (ECBAM) [54]. Traditionally, the GAU module replaces the decoder part's bilinear interpolation up-sampling, leading to enhanced segmentation accuracy and higher quality up-sampling.

3.6.1. Enhanced DeepLabV3+ Model

In medical image segmentation, the following are the significant shortcomings of the traditional DeeplabV3+ model [9]: omission of fine targets; incorrect judgment; nulling; an excessively long training period and a slow rate of network convergence; an excessive amount of DeeplabV3+ network parameters; and a worse segmentation effect for targets with smaller sizes. Considering the inadequacies mentioned above, the following changes are made in this paper: First, improvements are made to the Xception backbone network. Second, after the ASPP module is set, the ECBAM is confirmed experimentally to determine a set of optimal null rates. Lastly, the GAU module is employed in place of the fusion module, using the original up-sampling with the decoder portion. In Figure 8, the EDeepLabV3+ model is displayed.

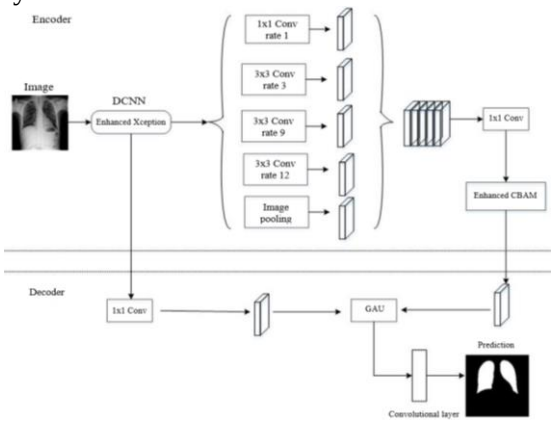

Figure 8. The structure of the EDeepLabV3+ model.

3.6.2. Enhancement of the Xception Backbone Network

The Xception model [55] requires a substantial amount of computational effort due to its numerous parameters and complex computational procedures. In comparison, Xception requires a greater amount of time and processing resources throughout the training and inference stages. As the three 2×2 average pooling layers are added to the Exit flow to reduce training and computation times, the average pooling layer converts local features into global features. With a wider medical imaging field, the feature map's resolution can be gradually decreased, allowing the model to gather more contextual data. Because lung tumors can be widely distributed in terms of size and shape throughout an image, this is significant for lung disease segmentation tasks. During segmentation, preserving every detail and the original resolution of the features is not necessary. Because lung tumor regions are typically large and distributed, they serve as targets. Since the tumor region's border is generally hazy, it is possible to make the feature map's boundary slightly smoother and blurrier by using an average pooling layer, thereby improving the continuity and robustness of the segmentation result. Figure 9 depicts the enhanced Xception model.

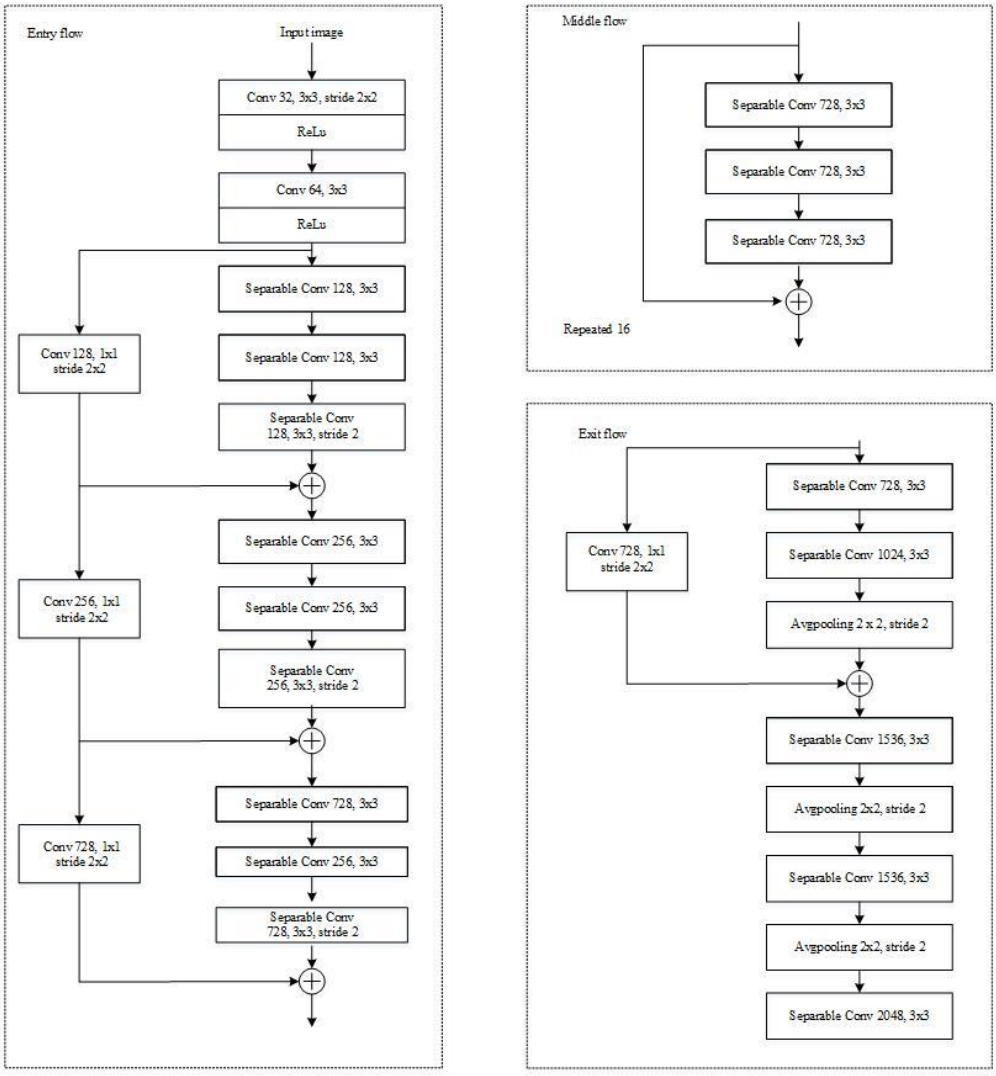

Figure 9. Enhanced Xception backbone network model.

3.6.3. Enhancement of Convolutional Block Attention Module (ECBAM)

The ASPP module is not very effective at capturing channel information; semantic information is usually captured in various spatial dimensions. An ECBAM module is added beneath the ASPP module to enhance the model's capacity. The ECBAM module is illustrated in the figure 10 It incorporates the attention adjustment's modified high-level features while keeping the original feature maps' low-level features. By introducing additional sophisticated, discriminating semantic data while preserving the original image's features and their low-level semantic data, it enables the gradient to spread directly to earlier layers. It enhances feature representation by introducing short-circuit connections. This facilitates efficient gradient propagation and optimization while also helping to alleviate the gradient vanishing problem.

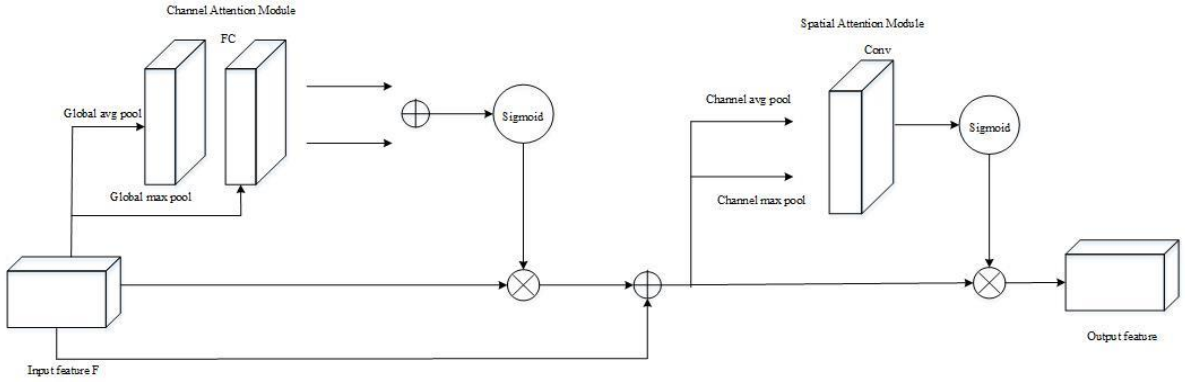

Figure 10. The structure of the ECBAM module.

3.6.4. Global Attention Upsample (GAU) Module

Accurately identifying the infected region boundary depends on global context information, and it is also necessary for appropriate region segmentation in lung disease segmentation assignments. The global context information may not be adequately utilized by traditional up-sampling techniques (such as bilinear interpolation), which could lead to the disappearance of detailed information in the feature map. However, by incorporating a global attention mechanism, the contextual dependencies can be captured more accurately at a distance using the GAU module. Increasing the up-sampling effect, feature comprehension, and boundary accuracy improves the feature map representation. The GAU model structure is depicted in Figure 11.

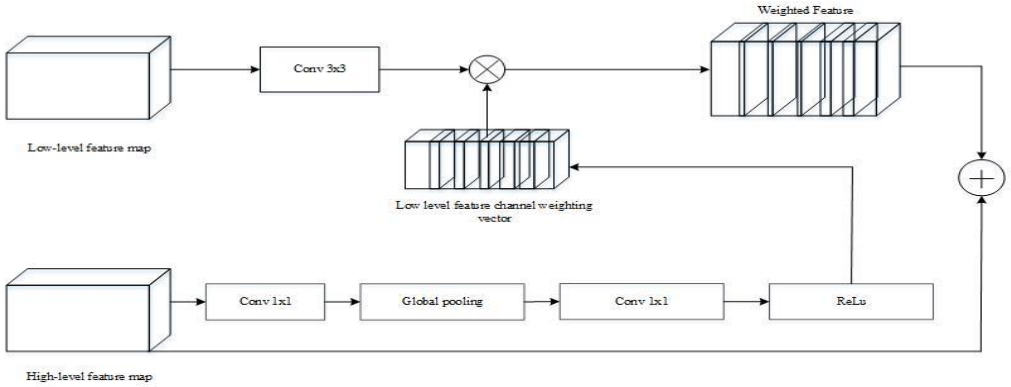

Figure 11. The structure of the GAU module.

3.6.5. Cross-Entropy Loss Function

Since there are several classes in the lung disease segmentation setup, the categorical cross-entropy loss function [24] is employed. One popular and extensively used loss function that has performed well is the categorical cross-entropy loss.

To ensure that lung disease types are appropriately trained and classified, this imbalance problem can be effectively addressed by modifying the category weights or implementing specific category balancing algorithms using this loss function. Among the actual labels and the prediction outcomes, the cross-entropy loss function is used to reduce the difference. The lung tumor region segmentation is the task goal that it implicitly targets, enabling the model to more fully understand the boundaries and distinctive features of the tumor area and its background.

The loss function formula given as Equation (2), CE_{loss} represents the categorical cross-entropy loss function.

$$CE_{loss} = -\frac{1}{N}\sum_{n=1}^{N}\sum_{c=1}^{C} l_c^{(n)} \bullet log\left(p_c^{(n)}\right) \quad (2)$$

The sample's number is denoted as *N*, and the number of categories is expressed as *C*. Sample *n*, which has undergone One-hot Encoding, is represented by the true label, $l_c^{(n)}$. Sample n for category *c* is represented by the probability $p_c^{(n)}$.

4. Result and Discussion

The empirical assessment of the proposed approach is presented in this section. This section describes the implementation environment and the dataset utilized in the experiment, as well as the evaluation measures that were utilized for evaluating the models' performance. An in-depth analysis of the experimental data is performed to assess the efficacy of the proposed approach, examine the influence of various variables on its operation, and explore its potential applications. The multi-class lung disease dataset is a publicly available

resource that we exploited for this research.

4.1. Experimental Settings

Utilizing a 16 GB of RAM with nvidia quadro RTX 5000 GPU, the experiment was conducted. The python programming language is used for analysis. Our model makes use of several essential libraries and technologies, including keras, TensorFlow, pennylane, and NumPy [11].

4.2. Hyper-parameter Settings

In the proposed research, nearly all hyperparameters are automatically optimized using the Adam optimizer [36], which adaptively adjusts the network's learning rates to ensure improved generalization and faster convergence. The following hyperparameters were chosen to achieve dependable performance in both segmentation (EDeepLabV3+) and classification (EResNet50V2), as indicated in Table 5.

Table 5. The model's hyper-parameters.

Parameters	Classification (Values)	Segmentation (Values)
Input Dimension	224 ×224	224 ×224
Learning Rate	0.001	0.001
Number of Epochs	100	100
Output dimension	224	224
Loss	Categorical cross-entropy loss function	Dice loss function
Maximum iteration	200	200
Batch Size	32	32
Dropout Rate	0.5	0.5

To reduce computational complexity and standardize the input size, all images were reduced to 224 × 224 pixels. For medical imaging tasks, CNN-based models (such as ResNet and VGG) frequently use this dimension, which enables efficient feature extraction.

The model's weight updates during training are determined by the learning rate. To avoid divergence (too high) and slow learning (too low), a value of 0.001 was selected since it strikes a fair compromise between convergence speed and stability.

The number of epochs is the number of times the model processes the entire dataset. One hundred epochs was enough to achieve convergence without overfitting, according to validation performance.

To ensure pixel-level mapping between the input image and the segmented region, the output mask was kept at 224 × 224 to match the input dimension throughout the segmentation process.

The Categorical Cross-Entropy loss function is used for multi-class classification issues because it efficiently penalizes inaccurate predictions across several categories.

To improve segmentation accuracy by directly optimizing the overlap between predicted and ground-truth regions, the Dice loss function is selected for segmentation tasks.

To preserve computational efficiency and ensure sufficient updates for convergence, the maximum number of iterations per epoch was set at 200.

To balance training stability and memory efficiency, a batch size of 32 was employed. Compared to batch sizes that are either too small or too large, this reasonable size facilitates the production of smoother gradient updates.

By randomly turning off 50% of neurons during training, dropout was used at a rate of 0.5 to improve model generalization by reducing overfitting.

4.3. Performance Measures

Using several evaluation metrics, the proposed deep learning models' ability to accurately identify regions of interest in a chest radiograph is evaluated. The number of wrongly identified background pixels is represented by FN, the number of mistakenly identified infected pixels is represented by FP, the number of correctly identified background pixels is indicated by TN, and The number of successfully recognized infected pixels is represented by TP. The five evaluation measures utilized for infection detection are accuracy, F1-score, recall, and precision [28]. Conversely, the IoU and DSC are used to evaluate the segmentation of infections.

$$Accuracy = \frac{(TN + TP)}{TN + FP + FN + TP} \tag{3}$$

$$Pr\,e\,cision = \frac{TP}{(FP + TP)} \tag{4}$$

$$Sensitivity/\,Re\,c\,all = \frac{TP}{(FN + TP)} \tag{5}$$

$$F1 - Score = 2 \times \frac{(Pr\,e\,cision \times Re\,c\,all)}{(Pr\,e\,cision + Re\,c\,all)} \tag{6}$$

Two segmentation parameters are frequently employed to evaluate the level of precision between the expected masks and the ground truth [42]. First, we have the Dice Similarity Coefficient (DSC), which indicates the number of pixels in each of the two masks that overlap and the total number of pixels. Between the ground truth and predicted masks, the percentage of common pixels, about the pixels that belong to either mask, is measured by the second parameter, called Intersection over Union (IoU).

$$DiceCoefficient = \frac{2 * |A \cap B|}{|A| + |B|} \tag{7}$$

$$Inter\,sec\,t\,ionoverUnion = \frac{|A \cap B|}{|A \cup B|} \tag{8}$$

Where the ground truth mask's pixel number is represented as A and the predicted mask's pixel number is represented as B.

4.4. Experimental Results

A thorough multi-class CXR image classification visualization is shown in Figure 12. By acquiring discriminative features from CXR, the EResNet50V2

can classify a variety of lung disorders, including viral Pneumonia, tuberculosis, lung opacity, Fibrosis, COVID-19, and normal lung states. The model's ability to identify intricate patterns related to various diseases is made possible by the deep residual layers, which enable precise classification. The EResNet50V2 model can help physicians understand the entire scope of lung disorders by providing a comprehensive view of how diseases are distributed throughout the lungs. Large-scale screening programs can benefit from the integration of the EResNet50V2 model into automated screening systems, which can consistently and quickly categorize lung diseases. By fine-tuning the decision boundaries between various lung disease classes, max-pooling layers enhance the model's capacity to discern between related diseases. Reducing overfitting with the dropout layer helps the model generalize better to data on lung diseases that have not yet been observed. Layers of batch normalization normalize each layer's inputs to minimize internal covariate shifts. This accelerates training and enables the use of higher learning rates, which in turn accelerates convergence.

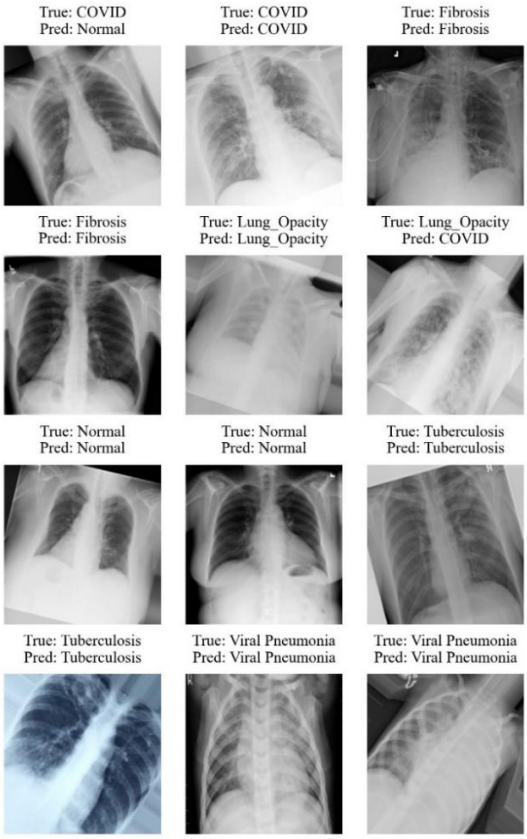

Figure 12. The classified outputs of the proposed research.

Because the proposed EDeepLabV3+ model can more precisely segment small, subtle anomalies, it can be used to identify lung diseases in their early stages. Accurate segmentation by EDeepLabV3+ for various lung disorders can aid in preoperative planning by pinpointing the exact position and boundaries of tumors, enabling more targeted therapies. The EDeepLabV3+ model demonstrates a remarkable capacity to precisely identify infected pixels while simultaneously reducing the number of false positives. Its remarkable precision and recall measures demonstrate its effectiveness in precisely identifying and segmenting the appropriate locations. In lung disease segmentation, the proposed model's superior performance is indicated by its Dice Similarity Coefficient (DSC) score of 98.67% and IOU score of 97.54% respectively.

The segmentation results of the proposed research are given in Figure 13. From each class, the infected sample X-ray images are shown in Figure 13 in the first row. In the second and third rows, the ground truth masks and the predicted masks are displayed. Both under- and over-segmentation may occur when segmenting the affected area of the lungs. It can be challenging for the model to establish a strong segmentation boundary when there is under-segmentation, as this can lead to information loss. Nonetheless, since no essential data is lost in the event of over-segmentation, the affected area can still be rebuilt. When compared to the baseline U-Net, the depicted results show that the EDeepLabV3+ model efficiently highlights the infection, closely aligning with the ground truth, while minimizing over-segmentation.

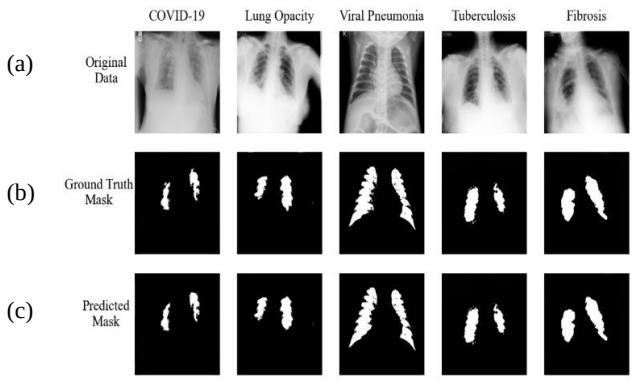

Figure 13. Simulation results of real-time sample prediction (a) Original data samples (b) Ground truth mask (c) Predicted mask by the EDeepLabV3+ model.

4.5. Classification Performance

The proposed classification model's classification report is shown in Figure 14. With an extensive range of diseases, the model performed admirably, displaying good F1-score, precision, recall, and accuracy. Our proposed approach performed remarkably well across a comprehensive range of disorders, with accuracy values exceeding 99% for specific conditions. Its precision is demonstrated by the fact that it performed exceptionally well in recognizing conditions such as COVID (100%), viral pneumonia (100%), tuberculosis (100%), fibrosis (100%), normal (99%), and lung opacity (100%). Additionally, the model demonstrated good recall rates for viral pneumonia (100%), and normal (100%). The lung opacity F1-score comes in second at 99%, and the tuberculosis F1-score at 100%. The proposed classification (EResnet50V2) model yielded overall

results of 99.33%, 99.83%, 99.33%, and 99.47% for F1-score, precision, recall, and accuracy, respectively. These remarkable findings demonstrate that the model is a powerful tool for medical image analysis, as it can accurately and consistently diagnose a wide range of chest conditions.

```
Accuracy: 0.9947313666343689
659/659 ━━━━━━━━━━━━━━━━━━━━ 1s 2ms/step
                precision    recall  f1-score   support

         COVID       1.00      0.99      0.99      2884
      Fibrosis       1.00      0.99      0.99      1347
   Lung_Opacity      1.00      0.99      0.99      4818
        Normal       0.99      1.00      0.99      8142
   Tuberculosis      1.00      0.99      1.00      2807
Viral Pneumonia      1.00      1.00      1.00      1070

      accuracy                           0.99     21068
     macro avg       1.00      0.99      1.00     21068
  weighted avg       0.99      0.99      0.99     21068
```

Figure 14. The classification report of the proposed model (EResNet50V2).

4.6. Accuracy and Loss Curves

For training and validation, the accuracy and loss curves of the proposed classification model are displayed in Figure 15. Figure 15-a) shows how well our proposed model performed during training for multi-class classification of lung diseases. Over 100 epochs, the training accuracy, represented by the blue line, improves from 0.53 to 0.99, while the validation accuracy, represented by the red line, improves from 0.51 to 0.99.52. Both the validation and training sets demonstrate that the proposed model performs well, indicating that it has acquired the ability to categorize images correctly.

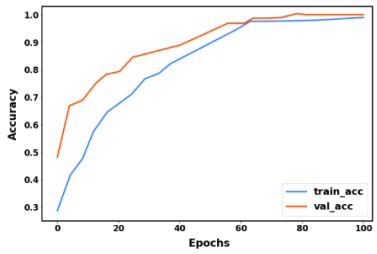

a) Accuracy curve.

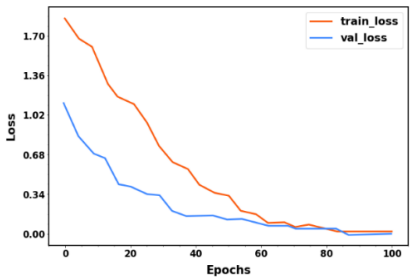

b) Loss curve for training and validation.

Figure 15. Comparing accuracy vs epochs.

Figure. 15-b) displays the loss during 100 epochs of training and validation. The blue line represents the training loss, while the red line represents the validation loss. The model achieves a minimum validation loss of 0.05 and a minimum training loss of 0.03. Despite having a very small number of parameters, all classes seem to have been distinguished by our proposed approach.

According to our research, the EResNet50V2 model efficiently reduces the size of larger models without compromising functionality. To perform similarly to larger models, it is possible to train models with fewer parameters by utilizing our distillation architecture, enabling lower computational expenses and faster inference times.

4.7. Confusion Matrix for Lung Disease Classification

Additionally, the confusion matrix is used to evaluate the classification performance [28]. For all lung disease types, the proposed classifier (EResNet50V2) consistently generates higher true positive predictions while maintaining a lower rate of false predictions across each category, as shown in the confusion matrix in Figure 16. This indicates that the model is not biased towards any particular disease class and shows that it is capable of accurately predicting all classes. 1443 COVID-19 cases were correctly recognized using our proposed EResNet50V2 model, although 2 cases were incorrectly categorized as Fibrosis, and 2 cases were incorrectly classified as opacity and tuberculosis. The proposed algorithm correctly detected 1211 cases of opacity from radiographs, misclassifying 4 cases as COVID-19, 2 cases as Pneumonia, and 4 cases as normal. The EResNet50V2 model correctly detects 9118 cancer-infected X-rays out of 9146 chest radiographs for lung cancer. Additionally, our proposed model accurately predicted the precise class designation of every non-infected case.

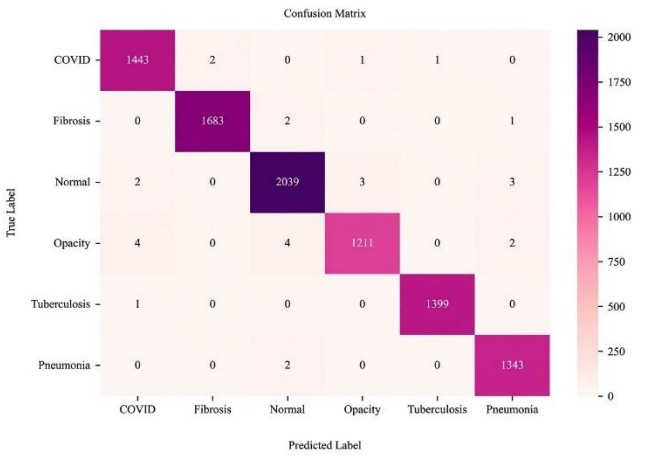

Figure 16. The confusion matrix of the proposed (EResNet50V2) model for classification.

4.8. Receiver Operating Characteristics (ROC) Curve

Figure 17 shows the ROC curves with AUC values for each class. Based on this illustration, our proposed

EResNet50V2 model consistently achieved an optimal accuracy of more than 99% across all lung disease categories. This demonstrates that the model can accurately and consistently predict a variety of lung diseases. From the ROC curves, our proposed model can be trusted to identify true positives, making it particularly useful in situations requiring precision, such as medical diagnostics, where the expense of false positives is intolerable.

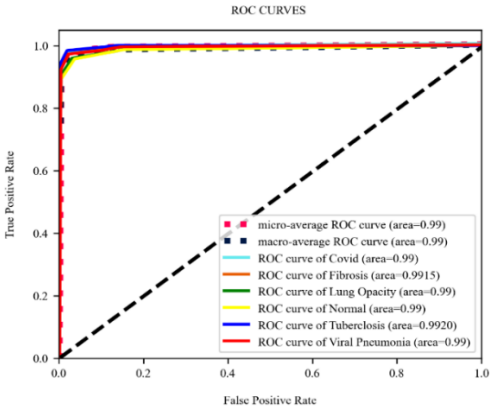

Figure 17. ROC curve of the proposed EResNet50V2 model.

4.9. Comparison with the State-of-the-Art Techniques

Our primary objective in this section was to compare our research with the existing literature. A comparison between previous research and our proposed approach is presented in Table 6, which evaluates variables such as F1-score, recall, precision, and accuracy. When compared to other recent models, such as Random Forest [52], ChestCovidNet [43], DWTMBConvNet [7], and CNN-HBOA [6], the proposed model (EResNet50V2) performs better. The best results for each performance metric are highlighted in bold.

For the multi-classification of lung diseases, the proposed (EResNet50V2) model classifies CXR images into COVID-19 Pneumonia, lung opacity, Fibrosis, viral pneumonia, normal, and tuberculosis classes, achieving an accuracy of 99.47%, an F1-score of 99.33%, a recall of 99.33%, and a precision of 99.83%. The detrimental effects of the classification process and the overfitting problem of the network are mitigated by the proposed enhanced models, which improve the classification and segmentation process. The inter-scale heterogeneity of the disease's features is efficiently extracted by the proposed method. Moreover, the categorization results of the proposed model are enhanced. The multi-class lung diseases can be pre-screened and automatically recognized by using the proposed models with exceptional classification accuracy. The qualities and methods suggested are considered suitable when various classifiers demonstrate reliable effectiveness in classification overall measures. As a result, the proposed method is labour-intensive, easy to use, enables remote patient monitoring, may detect lung conditions early, and is highly effective.

The segmentation performance of the proposed model (EDeepLabV3+) is analyzed by comparing its performance results with those of existing models, as shown in Table 7. The best results for each performance metric are highlighted in bold. With a dice coefficient of 98.67%, the integrated features of the proposed EDeepLabV3+ model outperform the baseline U-Net [20] model by 8.13%. Moreover, its IoU of 97.54% is 6.51% greater than that of the U-Net model. For lung disease segmentation, these results repeatedly show that the EDeepLabV3+ model outperforms other recently developed models. Additionally, the results of the proposed model (EDeepLabV3+) are compared to those of PulmonU-Net [39], U-net++ [17], Modified Otsu-binarization [30], and ResUNet [35], the proposed EDeepLabV3+ model can handle complex boundaries and small structures, as well as enhanced boundary detection and accurate boundary delineation during segmentation.

Table 6. Comparison of the previous state-of-the-art method's results with the proposed method's results for multi-class lung disease classification.

Reference	Year	Classes	Method	Accuracy (%)	Precision (%)	Recall (%)	F1-Score (%)
Yadav *et al*. [52]	2024	COVID-19, pneumonia, or tuberculosis	Random forest	98.03	98.42	97.35	98.04
Ullah *et al*. [45]	2024	COVID-19, normal, pneumonia, and lung opacity	ChestCovidNet	98.12	95.75	95.75	95.75
Bhosale *et al*. [7]	2024	normal, non-Covid-19 viral pneumoni, tuberculosis, bacterial pneumonia, and Covid-19.	DWTMBConvNet	95.5	96.2	95.5	98.9
Askr *et al*. [6]	2024	Lung opacity, COVID, normal, and pneumonia	CNN-HBOA	99.25	99.25	99.03	99.16
Proposed approach		Lung opacity, normal, Pneumonia, viral pneumonia, tuberculosis, and COVID-19	EResNet50V2	99.47	99.83	99.33	99.33

Table 7. Comparison of the previous state-of-the-art method's results with the proposed method's results for lung disease segmentation.

Reference	Year	Methods	IOU (%)	DSC (%)
Ishwerlal *et al*. [20]	2024	Unet	91.03	90.54
Shyni *et al*. [39]	2024	PulmonU-Net	88.3	94.25
Gite *et al*. [17]	2023	Unet++	95	
Nitha Vinod. [30]	2024	Modified otsu binarization	95	95.5
Sayeed *et al*. [35]	2024	ResUNet	94.51	96.33
Proposed approach		EDeepLabV3+	97.54	98.67

4.10. Statistical Significance Analysis

A statistical significance analysis was performed for both the segmentation findings (Table 7) and classification results (Table 6) to guarantee the validity of the stated improvements. A paired t-test was used to compare the competing approaches with the proposed EResNet50V2 model in terms of classification metrics over the same datasets. When compared to ResNet50

and modified VGG-19, the accuracy values reveal $p<0.01$, indicating that the improvements made by the proposed method are statistically significant. In particular, ResNet50 (mean=97.17%, 95% CI [96.12%, 98.01%]) and Modified VGG-19 (mean = 98.88%, 95% CI [98.04%, 99.36%]) were both substantially less accurate than the proposed model (mean=99.47%, 95% CI [98.93%, 99.83%]). The consistency of increases across different evaluation measures was confirmed by similar trends for precision, recall, and F1-score, all of which produced statistically significant differences with $p<0.05$.

The Wilcoxon signed-rank test was used to assess DSC and IoU scores for segmentation measures. In comparison to UNet++(DSC=94.21%, 95% CI [93.35%, 95.07%], $p<0.01$) and DeepLabV3+(DSC=92.85%, 95% CI [92.03%, 93.67%], $p<0.001$), the proposed EDeepLabV3+ model achieved a DSC of 97.56% (95% CI [96.84%, 98.28%]) and an IoU of 98.76% (95% CI [97.92%, 99.34%]). These findings suggest that the superior performance of the proposed segmentation framework is not due to random variation, but is statistically significant.

Overall, a 95% confidence level was used for all statistical tests. P-values<0.01 were deemed very significant, and improvements with p-values<0.05 were considered statistically significant. The findings demonstrate that, in comparison to state-of-the-art methods, the proposed models for lung disease classification and segmentation produce reliable and statistically supported performance improvements.

4.11. Discussion

This research analyzes prior multi-class lung disease detection and classification methodologies, in addition to presenting a novel approach to applying an enhanced deep learning model for image classification and segmentation tasks. The proposed research is implemented using the highly regarded deep learning-based EResNet50V2 and EDeepLabV3+ models, and the multi-class lung disease datasets are commonly utilized for the segmentation and classification process of lung diseases. When compared to other models, higher detection accuracy is achieved by the proposed model performance. Additionally, the convolutional and pooling layers of the Custom CNN model can collect selective data that each branch might have ignored. The input CXR image quality is enhanced by applying efficient pre-processing techniques such as noise reduction, normalization, and scaling. The affected tumor region in the lung is effectively segmented by the proposed EDeepLabV3+ model using efficient IOU and Dice scores. The CXR images are used to train the deep learning models (EResNet50V2-EDeepLabV3+) because they are of relatively high quality compared to the benchmark models.

The model's overall findings and analysis for the subtype classification reflect our perspective on using the EResNet50V2 model and adding extra layers, such as batch normalization, max pooling, and dropout layers, for extracting the efficient details of the images. The recall and F1-score of the testing dataset indicate better analytical performance. In contrast, the subtype classification is where the model excels the most, yielding higher values for all performance measures in each class. Overall, lung disease stages, when comparing the proposed model against all existing models, reveal higher accuracy.

The small lesion details are efficiently captured, and object boundaries are effectively separated across diverse data samples by the proposed research, as demonstrated by the real-time testing of the EDeepLabV3+ semantic segmentation model. Essential to the EDeepLabV3+ model is its capacity to maintain active neurons during training by utilizing the richness of multi-scale information.

98.67% dice coefficient and 97.54% IoU were attained by the proposed model. As a result, it is a good fit for lung disease segmentation due to its precision and consistency. The EDeepLabV3+ model is remarkable for its efficacy in highlighting diseases in all six groups; nevertheless, its limited capacity to distinguish between distinct infection categories may limit its usefulness in furnishing comprehensive diagnostic details. Future work on the EDeepLabV3+ model should focus on multi-class segmentation and provide a quantitative evaluation of infection severity within each class to enhance the model's utility.

4.12. Limitations and Future Research

Our automated approach has demonstrated better computational efficiency and accuracy on various datasets, handling noise, class fluctuations, and overlapping complications in CXR images with ease. This achievement suggests that medical imaging technology has a promising future. Future work on real-time CXR images will focus on expanding our dataset and subjecting our model to further tests. To improve dataset adaptability, we intend to investigate the possibilities of Generative Adversarial Networks (GANs) and Graph Convolutional Networks (GCNs). Furthermore, our goal is to develop a computer-aided decision-making system to assist physicians in treating patients with lung diseases. A significant improvement we make to our pipeline is to prioritize image segmentation, which may lead to better feature extraction. Our ultimate objective is to develop a real-time application for classifying lung diseases that enables the seamless integration of clinical and academic research, providing medical professionals with a more effective diagnostic tool.

5. Conclusions

A respiratory lung disease detection system is

developed in this research using the enhanced deep learning models EResNet50V2 for classification and EDeepLabV3+ for segmentation. First, the quality of the image is improved by removing unwanted noise using a Gaussian filtering-based pre-processing technique. As a result of less noise, the proposed classification model operates more efficiently. Subsequently, a new CCNN model extracts the required features to improve classification accuracy. This helps to achieve better performance and enhances the EResNet50V2 model's capacity for multi-class classification. The six categories of lung abnormalities and normal images were successfully categorized by the proposed EResNet50V2 model with a higher F1-Score (99.33%), recall (99.33%), precision (99.83%), AUC (99.05%), and accuracy (99.47%). The EDeepLabV3+ model effectively separates the affected area of the lung. The semantic segmentation model EDeepLabV3+ demonstrates its remarkable ability to capture small structural details and precisely define object boundaries across a variety of data samples through real-time testing. The key to EDeepLabV3+ is its ability to maintain active neurons throughout training by leveraging the richness of multi-scale details. 97.54% IoU and 98.67% DSC were attained with the EDeepLabV3+ model. The proposed deep learning model demonstrated its effectiveness in precisely classifying several lung diseases. The segmentation and classification comparison analysis reflects the competence of the proposed method in accurately classifying diseases.

Nevertheless, the proposed research only considers one combined dataset to evaluate the performance of the proposed model. Therefore, this problem will be addressed in the future by utilizing multiple datasets to demonstrate the efficacy of the proposed approach. In future research, appropriate characteristics to enhance the network model's functionality will be selected using a novel meta-heuristic feature selection scheme. Additionally, an effective deep-learning model will be developed to detect a variety of diseases, including kidney, eye, and brain diseases.

Acknowledgements

We declare that this manuscript is original, has not been published before, and is not currently being considered for publication elsewhere.

Availability of Data and Material:

The datasets analyzed during the current study are available from the corresponding author upon reasonable request.

Authors' Contributions

The author confirms sole responsibility for the following: study conception and design, data collection, analysis and interpretation of results, and manuscript preparation.

Ethics Approval

This material is the authors' own original work, which has not been previously published elsewhere. The paper reflects the authors' own research and analysis in a truthful and complete manner.

Reference

[1] Abhishek G., Singla A., and Eshwar D., "DICA-Net: Optimizing Chest X-Ray Classification with Attention U-Net and Pigeon Local Search," *Network Modeling Analysis in Health Informatics and Bioinformatics*, vol. 14, pp. 1-20, 2025. DOI:10.1007/s13721-025-00513-5

[2] Ali A., Wang Y., and Shi X., "Detection of Multi-Class Lung Diseases Based on Customized Neural Network," *Computational Intelligence*, vol. 40, no. 2, pp. e12649, 2024. https://doi.org/10.1111/coin.12649

[3] Almujally N., Mujtaba G., Alharbi S., Alshammari N., and Jalal A., "Swin Transformer-Enhanced UAV Surveillance: A Multi-Modal Feature Optimization for High-Precision Road Vehicles Detection," *The International Arab Journal of Information Technology*, vol. 23, no. 1, pp. 144-153, 2026. https://doi.org/10.34028/iajit/23/1/13

[4] Arora R., Rao G., Banerjea S., and Rajitha B., "MLDC: Multi-Lung Disease Classification Using Quantum Classifier and Artificial Neural Networks," *Neural Computing and Applications*, vol. 36, no. 7, pp. 3803-3816, 2024. https://doi.org/10.1007/s00521-023-09207-3

[5] Ashwini S., Arunkumar J., Prabu R., Singh N., and Singh N., "Diagnosis and Multi-Classification of Lung Diseases in CXR Images Using Optimized Deep Convolutional Neural Network," *Soft Computing*, vol. 28, no. 7, pp. 6219-6233, 2024. https://doi.org/10.1007/s00500-023-09480-3

[6] Askr H., Moawad M., Darwish A., and Hassanien A., "Multi-Class Deep Learning Model for Predicting Lung Diseases based on Honey Badger Algorithm," *International Journal of Information Technology*, vol. 17, no. 1, pp. 1147-1154, 2024. https://doi.org/10.1007/s41870-024-02046-y

[7] Bhosale R. and Yadav D., "Customized Convolutional Neural Network for Pulmonary Multi-Disease Classification Using Chest X-Ray Images," *Multimedia Tools and Applications*, vol. 83, no. 6, pp. 18537-18571, 2024. https://doi.org/10.1007/s11042-023-16297-7

[8] Cahyani D., Oktoviana L., Yasin M., Wahyuningsih S., and et al., "Lung Diseases Identification Using Hybrid Transfer Learning

and Bidirectional Long Short-Term Memory," *Bulletin of Electrical Engineering and Informatics*, vol. 14, no. 2, pp. 1418-1427, 2025. https://doi.org/10.11591/eei.v14i2.9114

[9] Chen H., Qin Y., Liu X., Wang H., and Zhao J., "An Improved DeepLabv3+Lightweight Network for Remote-Sensing Image Semantic Segmentation," *Complex and Intelligent Systems*, vol. 10, no. 2, pp. 1-11, 2024. DOI:10.1007/s40747-023-01304-z

[10] Chowdhury M. and Khandakar A., Kaggle, COVID-19 Radiography Dataset, https://www.kaggle.com/datasets/tawsifurrahman/covid19-radiography-database, Last Visited, 2024.

[11] Dandu R., Deepa B., and Murthy M., "Convolutional Neural Networks Framework for the Early Classification and Detection of Melanoma Skin Cancer," *SN Computer Science*, vol. 5, no. 5, pp. 1-14, 2024. https://doi.org/10.1007/s42979-024-02937-8

[12] Dawood H., Nawaz M., Ilyas M., Nazir T., and Javed A., "Attention-Guided CenterNet Deep Learning Approach for Lung Cancer Detection," *Computers in Biology and Medicine*, vol. 186, pp. 109613, 2025. https://doi.org/10.1016/j.compbiomed.2024.109613

[13] Deeplake, NIH ChestX-ray Dataset, https://datasets.activeloop.ai/docs/ml/datasets/nih-chest-x-ray-dataset/, Last Visited, 2024.

[14] Egala R. and Sairam M., "Multi-Layer Stacked Residual Coordinate Termite Alate Network for Multi-Class Lung Diseases Detection from Chest X-Ray Images," *Applied Soft Computing*, vol. 179, pp. 113393, 2025. https://doi.org/10.1016/j.asoc.2025.113393

[15] El-Ghandour M. and Obayya M., "Pneumonia Detection in Chest X-Ray Images Using an Optimized Ensemble with XGBoost Classifier," *Multimedia Tools and Applications*, vol. 84, pp. 5491-5521, 2025. https://doi.org/10.1007/s11042-024-18975-6

[16] Geethu Lakshmi G. and Nagaraj P., "Lung Cancer Detection and Classification Using Optimized CNN Features and Squeeze-Inception-ResNeXt Model," *Computational Biology and Chemistry*, vol. 117, pp. 108437, 2025. DOI:10.1016/j.compbiolchem.2025.108437

[17] Gite S., Mishra A., and Kotecha K., "Enhanced Lung Image Segmentation Using Deep Learning," *Neural Computing and Applications*, vol. 35, pp. 22839-22853, 2023. https://doi.org/10.1007/s00521-021-06719-8

[18] Guan C., Ai H., Wang W., and Singh R., "Multi-CNNs with Variational Information Bottleneck for Chest X-Ray Classification," *The Journal of Supercomputing*, vol. 81, no. 13, pp. 1-22, 2025. https://doi.org/10.1007/s11227-025-07767-w

[19] Hu W., Yang S., Guo W., Xiao N., and et al., "STC-UNet: Renal Tumor Segmentation Based on Enhanced Feature Extraction at Different Network Levels," *BMC Medical Imaging*, vol. 24, no. 179, pp. 1-14, 2024. https://doi.org/10.1186/s12880-024-01359-5

[20] Ishwerlal R., Agarwal R., and Sujatha K., "Lung Disease Classification Using Chest X-Ray Image: an Optimal Ensemble of Classification with Hybrid Training," *Biomedical Signal Processing and Control*, vol. 91, pp. 105941, 2024. https://doi.org/10.1016/j.bspc.2023.105941

[21] Karmakar M., Hota A., and Nag A., "Convolutional Neural Network (CNN) and Federated Learning-Based Approach for Lung Disease Detection," *Iran Journal of Computer Science*, vol. 8, pp. 2387-2408, 2025. https://doi.org/10.1007/s42044-025-00320-1

[22] Kordnoori S., Sabeti M., Mostafaei H., and Banihashemi S., "LungXpertAI: A Deep Multi-Task Learning Model for Chest CT Scan Analysis and COVID-19 Detection," *Biomedical Signal Processing and Control*, vol. 99, pp. 106866, 2025. https://doi.org/10.1016/j.bspc.2024.106866

[23] Kumar S. and Bhowmik B., "EffiCOVID-Net: A Highly Efficient Convolutional Neural Network for COVID-19 Diagnosis Using Chest X-Ray Imaging," *Methods*, vol. 240, pp. 81-100, 2025. https://doi.org/10.1016/j.ymeth.2025.04.008

[24] Latha D. and Mahesh T., "Feature-Driven Breast Cancer Classification via Hybrid Model Using Mammogram Images," *Journal of Medical Engineering and Technology*, vol. 49, no. 7, pp. 276-292, 2025. https://doi.org/10.1080/03091902.2025.2530938

[25] Malik H., Anees T., and Din M., "BDCNet: Multi-Classification Convolutional Neural Network Model for Classification of COVID-19, Pneumonia, and Lung Cancer from Chest Radiographs," *Multimedia Systems*, vol. 28, no. 3, pp. 815-829, 2022. DOI:10.1007/s00530-021-00878-3

[26] Munawwar S. and Rao P., "An Efficient Deep Learning Based Multi-Level Feature Extraction Network for Multi-Modal Medical Image Fusion," *The International Arab Journal of Information Technology*, vol. 22, no. 3, pp. 429-447, 2025. https://doi.org/10.34028/iajit/22/3/2

[27] Mutukuru R., Rajesh A., Ponduri V., Ahammed J., and Kothala L., "Transformer-Based RT-DETR Framework for Accurate Chest X-ray Disease Detection," *IRBM*, vol. 46, no. 6, pp. 100912, 2025. https://doi.org/10.1016/j.irbm.2025.100912

[28] Naeem A., Malik H., Din M., Sadeghi-Niaraki A., and et al., "Skindwnet: A Novel Deep Learning Model for Multi-Class Classification of Skin Cancers Using Dermoscopic Images," *Multimedia*

Systems, vol. 31, no. 314, pp. 1-28, 2025. https://doi.org/10.1007/s00530-025-01952-w

[29] Nayantara P., Kamath S., Kadavigere R., and Manjunath K., "Automatic Liver Segmentation from Multiphase CT Using Modified Segnet and ASPP Module," *SN Computer Science*, vol. 5, no. 4, pp. 1-18, 2024. https://doi.org/10.1007/s42979-024-02719-2

[30] Nitha V. and Vinod S., "Novel CEFNet Framework for Lung Disease Detection and Infection Region Identification," *Biomedical Signal Processing and Control*, vol. 9, pp. 106624, 2024. https://doi.org/10.1016/j.bspc.2024.106624

[31] Rao G., Rajitha B., Srinivasu P., Ijaz M., and Wozniak M., "Hybrid Framework for Respiratory Lung Diseases Detection Based on Classical CNN and Quantum Classifiers from Chest X-Rays," *Biomedical Signal Processing and Control*, vol. 8, no. 8, pp. 105567, 2024. https://doi.org/10.1016/j.bspc.2023.105567

[32] Rashad M., Alebiary D., Aldawsari M., El-Sawy A., and AbuEl-Atta A., "CCNN-SVM: Automated Model for Emotion Recognition Based on Custom Convolutional Neural Networks with SVM," *Information*, vol. 15, no. 7, pp. 1-16, 2024. https://doi.org/10.3390/info15070384

[33] Samee N., Houssein E., Saber E., Hu G., and Wang M., "Integrated Deep Learning-Based IRACE and Convolutional Neural Networks for Chest X-Ray Image Classification," *Knowledge-Based Systems*, vol. 329, pp. 114293, 2025. https://doi.org/10.1016/j.knosys.2025.114293

[34] Satapathy S., Cho S., Mishra S., Sah S., and Mohanty S., "A Federated Learning Approach for Classifying Chest Diseases from Chest X-Ray Images," *Biomedical Signal Processing and Control*, vol. 100, pp. 107107, 2025. https://doi.org/10.1016/j.bspc.2024.107107

[35] Sayeed A., Khansur N., Srizon A., Faruk M., and et al., "An Effective Screening of COVID-19 Pneumonia by Employing Chest X-Ray Segmentation and Attention-Based Ensembled Classification," *IET Image Processing*, vol. 18, no. 9, pp. 2400-2416, 2024. https://doi.org/10.1049/ipr2.13106

[36] Shariff V., Paritala C., and Ankala K., "Optimizing Non-Small Cell Lung Cancer Detection with Convolutional Neural Networks and Differential Augmentation," *Scientific Reports*, vol. 15, no. 15640, pp. 1-27, 2025. https://doi.org/10.1038/s41598-025-98731-4

[37] Sharma V., Nillmani., Gupta S., and Shukla K., "Deep Learning Models for Tuberculosis Detection and Infected Region Visualization in Chest X-Ray Images," *Intelligent Medicine*, vol. 4, no. 2, pp. 104-113, 2024. https://doi.org/10.1016/j.imed.2023.06.001

[38] Shastri A., Prajapati Y., Katariya H., Paliwal M., and Sabale K., "Enhancing Clinical Outcomes Using Deep Learning Solution for Accurate Lung Cancer Classification," *Sensing and imaging*, vol. 26, pp. 1-19, 2025. https://doi.org/10.1007/s11220-025-00548-y

[39] Shyni H. and E C., "Pulmonu-Net: A Semantic Lung Disease Segmentation Model Leveraging the Benefit of Multi-Scale Feature Concatenation and Leaky Relu," *Automatika*, vol. 65, no. 2, pp. 641-651, 2024. https://doi.org/10.1080/00051144.2024.2314918

[40] Singh B. and Kumar P., "A Unified Framework for Lung Disease Screening Using Chest X-Ray Images," *Engineering Applications of Artificial Intelligence*, vol. 161, pp. 112073, 2025. https://doi.org/10.1016/j.engappai.2025.112073

[41] Srivastava R., Kumar N., and Sandhan T., "Binary Classification of Laryngeal Images Utilising ResNet-50 CNN Architecture," *Indian Journal of Otolaryngology and Head and Neck Surgery*, vol. 77, no. 2, pp. 644-651, 2025. DOI:10.1007/s12070-024-05202-9

[42] Tam W., Babyn P., and Alirezaie J., "Robust Lung Segmentation in Chest X-Ray Images Using Modified U-Net with Deeper Network and Residual Blocks," *Computer Methods and Programs in Biomedicine Update*, vol. 8, pp. 100211, 2025. https://doi.org/10.1016/j.cmpbup.2025.100211

[43] Timpano G., Veltri P., Vizza P., Cascini G., and Manti F., "Deep Learning-Based 3D and 2D Approaches for Skeletal Muscle Segmentation on Low-Dose CT Images," *Journal of Imaging Informatics in Medicine*, pp. 1-13, 2025. https://doi.org/10.1007/s10278-025-01646-9

[44] Truong T. and Do T., "Multimodal Approach for Lung Disease Classification: Fusing Chest X-Ray Images and Clinical Texts," *SN Computer Science*, vol. 6, pp. 607, 2025. https://doi.org/10.1007/s42979-025-04138-3

[45] Ullah N., Khan J., Almakdi S., Alshehri M., and et al., "ChestCovidNet: An Effective DL-based Approach for COVID-19, Lung Opacity, and Pneumonia Detection Using Chest Radiographs Images," *Biochemistry and Cell Biology*, vol. 104, pp. 1-16, 2024. DOI:10.1139/bcb-2023-0265

[46] Varadharajan I. and Rathinavelayutham S., "An Efficient Lung Disease Classification Using Dove Swarm Optimization Based Multi-Scale Faster-RCNN Model," *Evolving Systems*, vol. 16, no. 3, pp. 1-22, 2025. https://doi.org/10.1007/s12530-025-09708-7

[47] Vasudevan P. and Ekambaram C., "HYAQP: A Hybrid Meta-Heuristic Optimization Model for Air Quality Prediction Using Unsupervised Machine Learning Paradigms," *The International Arab Journal of Information Technology*, vol. 21,

no. 5, pp. 953-966, 2024. https://doi.org/10.34028/iajit/21/5/15

[48] Verma K., Sikka G., Swaraj A., Kumar S., and Kumar A., "Classification of COVID-19 on Chest X-Ray Images Using Deep Learning Model with Histogram Equalization and Lung Segmentation," *SN Computer Science*, vol. 5, pp. 1-15, 2024. https://doi.org/10.1007/s42979-024-02695-7

[49] Wei S., Hu Z., and Tan L., "Res-ECA-Unet++: An Automatic Segmentation Model for Ovarian Tumor Ultrasound Images Based on Residual Networks and Channel Attention Mechanism," *Frontiers in Medicine*, vol. 12, pp. 1589356, 2025. DOI:10.3389/fmed.2025.1589356

[50] Weli M. and Abdullah O., "Digital Image Noise Reduction Based on Proposed Smoothing and Sharpening Filters," *The Indonesian Journal of Computer Science*, vol. 13, no. 4, pp. 5001-5021, 2024. https://doi.org/10.33022/ijcs.v13i4.4151

[51] Wen M., Li C., Xue Y., Xu M., and et al., "YOFIR: High Precise Infrared Object Detection Algorithm Based on YOLO and Fasternet," *Infrared Physics and Technology*, vol. 144, pp. 105627, 2025. https://doi.org/10.1016/j.infrared.2024.105627

[52] Yadav S., Rizvi S., and Agarwal P., "Detection of Lung Diseases for Pneumonia, Tuberculosis, and COVID-19 with Artificial Intelligence Tools," *SN Computer Science*, vol. 5, pp. 1-18, 2024. https://doi.org/10.1007/s42979-024-02617-7

[53] Yang L., Wan Y., and Pan F., "Enhancing Chest X-ray Diagnosis with a Multimodal Deep Learning Network by Integrating Clinical History to Refine Attention," *Journal of Imaging Informatics in Medicine*, vol. 38, pp. 3568-3583, 2025. https://doi.org/10.1007/s10278-025-01446-1

[54] Ye Y., Chen Y., Wang R., Zhu D., and et al., "Image Segmentation Using Improved U-Net Model and Convolutional Block Attention Module Based on Cardiac Magnetic Resonance Imaging," *Journal of Radiation Research and Applied Sciences*, vol. 17, no. 1, pp. 100816, 2024. https://doi.org/10.1016/j.jrras.2023.100816

[55] Yilmaz E., Gorurgoz C., Kıs H., Canger E., and Oztaş B., "Forensic Dental Age Estimation with Deep Learning: A Modified Xception Model for Panoramic X-Ray Images," *Forensic Science, Medicine and Pathology*, vol. 21, no. 2, pp. 565-579, 2025. DOI:10.1007/s12024-025-00962-4

[56] Zou L., Li J., Chen H., Liang M., and et al., "MCG-Net: Medical Chief Complaint-Guided Multi-Modal Masked Content Pre-training for Chest Image Classification," *Expert Systems with Applications*, vol. 271, pp. 126660, 2025. https://doi.org/10.1016/j.eswa.2025.126660

Revathi Annam received the Bachelor's degree in Computer Science and Information Technology from JNTU University, Hyderabad in 2005, the master's degree in Computer Science Engineering from JNTU University in 2011 and pursuing doctorate degree in Computer Science Engineering from KLU University, Hyderabad. She is currently working as an Assistant Professor at the Department of Information Technology, VNR Vignana Jyothi Institute of Engineering and Technology, Hyderabad. Her research areas include Deep Learning, Machine Learning, Data Mining, Mobile Application Development and Mobile Security, etc.

Savadam Balaji is working as Associate Dean Academics, KL University, Hyderabad Campus, a Technocrat with Exposure to Industry, Academics and Research. His education is MTech and PhD in cyber forensics, with specific research interest in the field of Cyber Security and IoT. Having more than 28 years of teaching experience in various Engineering Colleges. He is also Principal investigator for AICTE-MODROBS project "Design of Embedded and VLSI Excellence Centre," worth Rs. 20 lakhs. Completed many Consultancy Projects and has organized many Conferences, Workshops and FDPs. Presently Guiding eight PhD Scholars under KL University and M. Tech Students in JNTUH and KLU. Published 30+ research papers in many reputed journals, conferences, one patent and 3 books. Recipient of two prestigious awards "Education Excellence Award-2020" and "Dr.A.P. J Abdul Kalam Pillars of India-22 Award".